Journal of Materials Chemistry B

ROYAL SOCIETY OF CHEMISTRY

PAPER

View Article Online
View Journal | View Issue

Cite this: J. Mater. Chem. B, 2026, 14, 1296

Non-cytotoxic, iodinated poly(ethylene oxide) (PEO) block-*co*-polymer contrast agents for computed tomography (CT) imaging

Mayson Whipple, [a] Barbara Christian,[b] Kendell M. Pawelec, [cd] Netsanet Waal, [a] D. Adam Lauver [b] and Robert C. Ferrier Jr. *[a]

Received 15th September 2025,
Accepted 22nd December 2025

DOI: 10.1039/d5tb02069g

rsc.li/materials-b

Medical imaging techniques like X-ray, magnetic resonance imaging (MRI), and computed tomography (CT) rely on contrast agents to enhance the visibility of blood vessels, tissues, and organs, making them crucial for medical diagnoses. Contrast agents used clinically for CT are typically small molecules containing iodine, which are associated with nephrotoxicity, often require large doses that can disrupt thyroid function, have short half-lives, and are sometimes immunogenic. Loading/functionalization of larger molecules with iodine may attenuate X-rays similarly to small molecules, but at much lower concentrations, potentially mitigating the adverse effects of current contrast agents. To test this, iodinated poly(ethylene oxide) (PEO) was synthesized with varying amounts of iodine and structural features and examined for use as a contrast agent. First, 5 kg mol^{-1} PEG containing one terminal hydroxyl was reacted with trimethylaluminum to form a macroinitiator from which block-*co*-polymers consisting of PEO-*co*-poly(epichlorohydrin) (PECH) were synthesized with PECH blocks of 5, 15, and 30 kg mol^{-1}. The polymers were subsequently iodinated and characterized with ^{1}H NMR and ^{13}C NMR spectroscopy, size exclusion chromatography (SEC), and differential scanning calorimetry (DSC). X-Ray attenuation was found to be similar to that of iohexol, a conventional contrast agent. Further, we found that high molecular weight polymers were completely non-cytotoxic, unlike iohexol, with polymer size the dominating factor for cytotoxicity rather than iodine concentration. As such, these new materials hold promise as medical contrast agents.

Introduction

X-Ray imaging techniques are fundamental in modern medicine for safe, effective, and rapid diagnosis, in which X-ray photons are passed through the body to a detector to generate images of internal structures. Computed tomography (CT) utilizes X-ray radiography to obtain highly detailed, high-resolution images that provide structural information on soft tissue, bones, and blood vessels. CT scanners work by rotating a thin X-ray beam and detector around the patient, taking hundreds of X-ray images to be reconstructed into a three-dimensional image.[1] Compositional differences of various tissues (*i.e.*, soft tissue, bones, blood vessels) results in absorption and/or scattering of X-ray photons leading to a decrease in the X-ray intensity measured by the detector. This decrease in intensity is referred to as X-ray attenuation, measured in Hounsfield Units (HU). Differentiation of tissue is based on the degree of X-ray attenuation, with bones measuring over 1000 HU[2] and as a result high contrasted images of bones can be attained. In comparison, many soft tissues attenuate X-rays to a similar degree (between 0 and 50 HU)[3] and therefore cannot be easily discerned. Consequently, exogenous contrast agents are required to augment CT images for differentiation of soft tissues.

Elements of higher atomic number (Z) attenuate X-rays at high levels and, historically, iodine (Z = 53) has been incorporated into contrast media for clinical CT.[4] Today, nearly all available contrast agents are based on the modification of a triiodinated benzene ring with hydrophilic functional groups to facilitate solubility, classified as iodinated contrast agents (ICA).[5] Existing ICAs are either ionic or nonionic and monomeric or dimeric, with monomeric agents containing one triiodinated benzene ring and dimeric containing two.[6] ICAs with low (nonionic monomer ex. iohexol) or similar (nonionic dimer ex. iodixanol) osmolarity compared to human blood plasma have proven less toxic than high osmolarity agents.[6] Dimeric structures can fit higher concentrations of iodine per osmole,

[a] Department of Chemical Engineering and Materials Science, Michigan State University, East Lansing, MI, USA. E-mail: ferrier5@msu.edu
[b] Department of Pharmacology and Toxicology, Michigan State University, East Lansing, MI, USA
[c] Department of Radiology, Michigan State University, East Lansing, MI, USA
[d] Institute of Quantitative Health Science and Engineering, Michigan State University, East Lansing, MI, USA

allowing for optimal radiopacity at lower concentrations and thus lower osmolarity and toxicity.[7]

Existing contrast agents have been associated with adverse reactions, namely thyroid dysfunction, immune reactions, and nephrotoxicity. The mechanisms prompting adverse reactions are not fully understood; however, the high doses required for effective contrast is likely a contributing factor.[4] X-Ray attenuation increases linearly with iodine concentration and traditional small molecule ICAs require high dosing volumes to achieve effective contrast.[8] Existing ICAs introduce iodine in concentrations several hundred thousand times the recommended daily dose of iodine. High levels of free iodine in the body are associated with thyroid dysfunction and while contrast-induced thyroid dysfunction is relatively rare, excess exposure to iodine can induce permanent hyperthyroidism in some patients.[4] Further, direct toxicity on renal cells from existing, small molecule ICAs can cause contrast-induced nephropathy, a potentially life-threatening condition. The risk is highest in patients with prior renal dysfunction, diabetes, and intensive care patients.[9] Consequently, patients requiring critical diagnosis for treatment planning and monitoring of disease progression are unable to utilize contrasted CT, which may delay diagnosis and lead to poor treatment outcomes.

There is a clear need for novel contrast agents that (1) exhibit high X-ray attenuation at lower concentrations and (2) are non-cytotoxic, particularly to renal cells. Polymer-based contrast agents may be advantageous due to the unique properties afforded by polymers, such as biocompatibility, facile synthesis, and versatility in structural modification and functionalization.[10] Recent advances in polymeric drug delivery systems have been explored to improve biocompatibility, circulation time, and more efficient targeting through encapsulation and delivery of existing ICAs.[11,12] Other polymeric approaches aimed to form iodinated macromolecules *via* polymerization of iodinated monomers or functionalization of polymer backbones with iodine or iodinated compounds.[13–15] These strategies have highlighted the potential for polymeric contrast agents to overcome the drawbacks of existing ICAs; however, complex synthesis, low iodine content, moderate contrast, or low biodegradability and/or biocompatibility have limited their advancement to clinical use.

Aside from intravenous contrast agents, CT imageable probes have been incorporated into polymer-based biomedical devices to improve clinical assessment. While not generally iodine-based, these CT probes nonetheless consist of high Z materials and are often in the form of nanoparticles. For example, Pawelec *et al.* incorporated biocompatible tantalum oxide (TaO_x) nanoparticles into biocompatible polymer-based scaffolds.[16,17] They were able to monitor the degradation of the devices over time both *in vitro* and *in vivo* due to the contrast from the TaO_x. Other examples of nanoparticles for CT imaging are extant and they provide strong contrast.[18,19] However, there are concerns about the long- and short-term impacts to the patient of exposure to high Z nanoparticles, as well as scale-up and other clinically relevant factors.[20] Furthermore, compatibilizing nanoparticles with polymers, biomedical or otherwise, can be challenging[21,22] and may add additional modification and/or processing steps.

In this work, we set out to explore polyether materials as potential contrast agents. Polyethers, especially poly(ethylene oxide) (PEO), are commonly used for biomedical applications. However, PEO is largely non-functional. We sought to combine PEO with a functional polyether material, polyepichlorohydrin (PECH) to enable a tunable, high-contrast, and biocompatible polymer platform. This work explores this platform for biomedical imaging applications. Specifically, we created iodinated polymers from functional polyethers, which provide high tunability, high iodine content, and are non-cytotoxic. Block copolymers consisting of PEO and PECH were synthesized by chain extension polymerization from 5 kg mol^{-1} PEO and functionalized with iodine moieties. Iodinated polymers (PEO–PEI) were synthesized with iodine concentrations ranging from 29% to 90% by targeting increasing PECH block sizes of 5 kg mol^{-1}, 15 kg mol^{-1}, and 30 kg mol^{-1}. Polymer structures were characterized with nuclear magnetic resonance (NMR) spectroscopy, differential scanning calorimetry (DSC), and gel permeation chromatography (GPC). Micro-CT (μCT) imaging demonstrated high levels of X-ray attenuation can be achieved at 20× lower sample concentrations of PEO–PEI (low M_n & lowest iodine content) compared to conventional iohexol. ICP-MS analysis revealed iodine concentrations in the PEO–PEI case at similar levels to iohexol, even with the low concentration of the PEO–PEI molecules themselves, confirming the presence of iodine on the polymer chain. A predictive model for X-ray attenuation given polymer concentration at particular Cl to I conversion was generated to inform future design of iodinated polymers. Finally, cytotoxicity of PEO–PEI was assessed in human renal cells. Higher molecular weight PEO–PEI exhibited no cytotoxicity while lower molecular weight PEO–PEI was cytotoxic and exhibited behavior similar to that of iohexol. This work is a first step in developing these radiopaque polymer materials for biomedical imaging applications.

Experimental

Materials

Poly(ethylene glycol) methyl ether (PEO, average M_n 5000 g mol^{-1}), sodium iodide (NaI, ACS reagent, >99.5%), tetrabutylammonium bromide (TBAB, ACS reagent, >98%), 1,4-diazabicyclo-[2.2.2]octane (DABCO, ReagentPlus, >99%) trimethylaluminum solution ($AlMe_3$, 2.0 M in hexane), triethylamine (TEA, >99.5%), epichlorohydrin (ECH, >99.0%), dimethyl sulfoxide (DMSO, ACS reagent, >99.9%) and methyl ethyl ketone (MEK, ACS reagent, >99.0%) were purchased from Sigma-Aldrich and used as received. Hexanes (Sigma Aldrich, anhydrous, >99%) and benzene (Sigma Aldrich, anhydrous, >99.0%) were used for initiator/catalyst purification in the glovebox. Methanol (MeOH, Fisher, Certified ACS) and dichloromethane (DCM, Fisher, Certified ACS) were used for washing the polymers. $CDCl_3$ was purchased from Cambridge Analytica and used as a solvent for NMR spectroscopy. All air and moisture-sensitive reactions were prepared under a dry nitrogen atmosphere inside a glovebox. Epithelial cells (RPTEC/TERT1: ATCC

cat. No CRL-4031), DMEM-F12 medium (Cat no. 30-2006), and RPTEC Growth Kit (ATCC Cat no. ACS-4007) were purchased from ATCC for cytotoxicity assays. Gly-Phe-7-Amino-4-Trifluoromethylcoumarin (Cat no. 03AFC03310) was purchased from MP Biomedicals. White 384 well plates (Cat no. 3570) were purchased from Corning and Neo plate reader from BioTek Synergy. Iohexol, used as positive control for cytotoxicity assays, was purchased from TCI (cat no. I0903).

Characterization

NMR spectroscopy ^{1}H and ^{13}C NMR spectroscopy were performed on a Bruker Avance III HD 500 MHz NMR spectrometer at room temperature with chemical shifts reported in parts per million (ppm) and referenced using deuterated solvents residual peaks.

Size exclusion chromatography (SEC) was performed using a Tosoh EcoSEC Elite on THF with refractive index used for molecular weight determination. Calibration was performed using polystyrene standards in THF rather than PEG due to solvent incompatibility.

Differential scanning calorimetry (DSC) was performed on a TA250 instrument with a heating rate of 10 °C min^{-1} under an N_2 atmosphere.

Inductively coupled plasma mass spectroscopy (ICP-MS) was used to measure iodine content in solutions and was conducted at the quantitative bio element analysis and mapping (QBEAM) Center (Michigan State University). Samples were digested for 4 hours in HNO_3. After digestion, a liquid sample was added to a matrix consisting of 0.1% w/v EDTA, 2% v/v NH_4OH and 0.01% v/v Triton X-100 in water, with Gadolinium (Gd) ISTD.

Micro-computed tomography (CT) imaging. All tomography images were obtained using a PerkinElmer Quantum GX at 90 keV, 88 μA, with a 36 mm field of view at a 50 μm resolution. Scans were taken with 2 min scan time, corresponding to a step size: 0.11 degrees and exposure time per projection: 36 m s. Solutions of iodinated and non-iodinated polymers were prepared in DI water or DCM. Iohexol solutions were used as a positive control.

Statistics were performed using GraphPad Prism (v. 10.0.2). All data were analyzed *via* ANOVA, followed by Fisher's LSD test. Cytotoxicity results were analyzed by comparing the percent cell viability relative to the control. Nonlinear regression was performed to create best-fit curves. In all cases, $\alpha < 0.05$ was considered significant, with a 95% confidence interval. Data are presented as mean ± standard error.

Methods

Synthesis of trimethylaluminum and triethylamine adduct (NAl)

Synthesis of NAl catalyst was done according to prior work.[23] 6.35 mL of anhydrous hexanes and 2.0 M $AlMe_3$ in hexane (6.35 mL, 12.7 mmol) were added to a reaction vial charged with a stir bar in a dry nitrogen glovebox and cooled to −78 °C. Then, TEA (1.5 mL, 10.7 mmol) was added dropwise, and the solution was stirred and warmed to room temperature overnight. The desired product was crystallized by cooling, the solution to −40 °C and resultant crystals washed three times with anhydrous hexanes (3 by 5 mL) and dried *in vacuo*.

^{1}H NMR (500 MHz, $CDCl_3$) δ 2.80 (q, 6H), 1.18 (t, 9H), −0.89 (s, 9H). ^{13}C NMR (126 MHz, $CDCl_3$) δ 47.78, 9.20.

Synthesis of poly(ethylene oxide)-*co*-poly(epichlorohydrin) block copolymers (PEO–PECH)

In a dry nitrogen glovebox, poly(ethylene oxide) (5 kg mol^{-1}) (1 mmol, 5 g) was dissolved in anhydrous benzene in a reaction vial charged with a stir bar. 2.0 M trimethyl aluminum in hexane (1 mmol, 0.5 mL) was added dropwise and the solution was stirred overnight at room temperature. Then, NAl catalyst and epichlorohydrin were added to the vial in amounts corresponding to targeted molecular weights of 5, 15, and 30 kg mol^{-1} for the PECH block. For 5 kg mol^{-1} PECH block, 86.25 mg NaI and 2.5 g ECH was added. For 15 kg mol^{-1} PECH block 28.86 mg NAl and 7.5 g ECH was added. For 30 kg mol^{-1} PECH block, 14.43 mg NAl and 15 g of ECH was added. The solution was heated to 50 °C until the completion of the polymerization. The resulting polymers were purified by washing in water and methanol, centrifuged to isolate the polymer, and dried under vacuum. Polymers were characterized by ^{1}H and ^{13}C NMR spectroscopy, DSC, SEC.

^{1}H NMR (500 MHz, $CDCl_3$) δ 3.80–3.66 (bm, C**H**–C**H$_2$**Cl), 3.64–3.56 (bm, C**H$_2$**C**H$_2$** and C**H$_2$**CH–CH$_2$Cl).

^{13}C NMR (500 MHz, $CDCl_3$) δ 79.08 (t, –O–CH$_2$–**C**H(CH$_2$Cl)–O–), 70.59 (s, **C**H$_2$**C**H$_2$), 69.89–69.30 (bm, **C**H$_2$–CH–CH$_2$Cl), 43.65 (s, **C**H$_2$Cl).

Procedure for modifying PEO–PECH with iodine

Polymers (0.5 g) were dissolved in methyl ethyl ketone (MEK, 50 mL) in a vial charged with a stir bar. Tetrabutyl ammonium bromide (50 mg) was added, followed by sodium iodide in molar equivalent with the number of Cl pendants on PECH block (~0.8 g). Then, the solution was refluxed at 80 °C for 72 hours. Iodinated polymers were purified by dialysis in DI water and dried under vacuum. Resulting polymers were characterized by ^{1}H NMR spectroscopy, DSC, and SEC.

^{1}H NMR (500 MHz, $CDCl_3$) δ 3.80–3.66 (bm, C**H**–C**H$_2$**I), 3.64–3.56 (bm, C**H$_2$**C**H$_2$** and C**H$_2$** CH–CH$_2$I), 3.46–3.24 (bm, CH$_2$CH–C**H$_2$**I).

Cell culture and cytotoxicity assay protocol

Human renal proximal tubule epithelial cells (RPTEC/TERT1; ATCC Cat. no. CRL-4031) were maintained for at least one week in hTERT-immortalized RPTEC growth medium under standard culture conditions. Following this acclimatization period, cells were seeded into 384-well plates at a density of 6000 cells per well in a media volume of 50 μL per well and allowed to adhere overnight in a humidified incubator at 37 °C with 5% CO_2.

PEO–PEI or iohexol (positive control) stock solutions were prepared by dissolving powder in RPTEC/TERT1 media, which

was subsequently serially diluted 2-fold to generate a range of concentrations.

On the day of treatment, the culture medium was aspirated from each well and replaced with media containing PEO–PEI or iohexol at the indicated concentrations in triplicate. After 30 minutes of incubation, MP Biomedicals™ Gly-Phe-7-Amino-4-Trifluoromethylcoumarin (Cat. no. 03AFC03310) was added to the wells, followed by an additional incubation period.

Cell viability was assessed by measuring fluorescence using a BioTek Synergy Neo plate reader at one- and two-hours post-PEO exposure.

Results and discussion

Polyethers, like poly(ethylene oxide) (PEO), are biocompatible and tunable and therefore make for a potential platform for radiopaque polymers. Functionalization of polyethers with iodine may attenuate X-rays similar to small molecules, while also being less cytotoxic and facilitating stable incorporation into other biomedical materials. PEO itself has no functional groups along the backbone. Therefore, our material design centered on a block copolymer structure consisting of a biocompatible PEO block and a functional polyepichlorohydrin (PECH) block which could be easily modified with iodine as a post-polymerization step.

Block-*co*-polymers consisting of PEO and PECH were synthesized as precursors for tuning the polymer iodine content. Chain extension polymerization of epichlorohydrin (ECH) was performed using an NAl catalyst[23–25] and an aluminum alkoxide PEO macroinitiator, as shown in Scheme 1. Briefly, the macroinitiator was formed by reacting a commercially obtained PEO (average M_n of 5000 g mol^{-1}) containing one hydroxyl end group (commonly referred to as mPEG) with trimethylaluminum and stirring at room temperature overnight. NAl catalyst and epichlorohydrin were then added in amounts to target PECH blocks of 5000 g mol^{-1}, 15 000 g mol^{-1}, and 30 000 g mol^{-1}. ^{1}H and ^{13}C NMR spectroscopy were used to confirm copolymer structure and determine molecular weight. The resultant spectra and a detailed example calculation can be found in the SI (Fig. S1–S6). Ratios of PECH to PEO were determined based on the ^{1}H NMR spectra by setting the integration of the PEO peak at 3.64 ppm to 4 (accounting for the OCH_2CH_2 backbone), integrating both backbone peaks, subtracting by 4, and dividing by 5 (the number of protons in the PECH block). The relative amount of PECH could then be calculated based on the ratio of PECH to PEO. For example, the PECH:PEO ratio for target 5 kg mol^{-1} was 0.46 so relative PECH was calculated to be 0.32 (0.46/(1 + 0.46)). M_n of the PECH block was then calculated by finding the total number of repeat units (N), subtracting the N of PEO, and multiplying by the molecular weight of PECH repeat unit. PECH M_n were found to be 4872 g mol^{-1}, 15 556 g mol^{-1}, and 30 402 g mol^{-1} in good agreement with the target M_n. Polymerization details can be found in Table 1.

Table 1 Polymer characteristics

Sample	PECH M_n^{theo} (kg mol^{-1})	PECH M_n[a] (kg mol^{-1})	PECH M_n[b] (kg mol^{-1})	$Đ$	Iodine conversion (%)
PEO–PECH5	5	4.9	4.7	1.3	—
PEO–PECH15	15	15.6	16.3	2.2	—
PEO–PECH30	30	30.4	29.6	2.4	—
PEO–PEI5	5	6.2	—	—	27
PEO–PEI15	15	20.0	20.4	2.1	26
PEO–PEI30	30	60.3	32.3	1.9	92

[a] Determined from ^{1}H NMR. [b] Determined from SEC.

Copolymers were analyzed by SEC for further confirmation of molecular weights and determination of polydispersity ($Đ$). RI spectra can be found in the SI (Fig. S7). SEC revealed copolymers with M_n of 9693 g mol^{-1} and $Đ$ = 1.3 for the target PECH block of 5 kg mol^{-1}, 21 300 g mol^{-1} and $Đ$ = 2.2 for the target PECH block of 15 kg mol^{-1}, and 34 615 g mol^{-1} and $Đ$ = 2.4 for the target PECH block of 30 kg mol^{-1}. These results compare favorably to the molecular weights targeted and calculated by ^{1}H NMR spectra. The polydispersity increased with molecular weight, which was also observed in previous work from Keever *et al.*, albeit the PEO and PECH blocks were smaller than in this work.[26] Furthermore, this high $Đ$ at higher molecular weight may be due to the better solubility of the PECH block compared with the PEO block in THF (the GPC solvent). This is supported by the fact that when we replaced most of the Cl with I, we see a drop in the $Đ$, indicating this could be a solvent effect. Despite the relatively high $Đ$ from a synthetic polymer chemistry standpoint, biomedical polymers at similar $Đ$ are utilized medically.

Copolymers will be referenced throughout the rest of this manuscript according to the relative M_n of the PECH block (PEO–PECHX). For example, the copolymer with target PECH M_n of 5 kg mol^{-1} is referred to as PEO–PECH5. Iodinated copolymers will be referenced similarly except with PEO–PEIX, where X is the molecular weight of the PECH block.

DSC was performed on each polymer and truncated traces can be found in Fig. 1. Full DSC traces for each polymer can be found in the SI (Fig. S8–S10). The DSC revealed one T_g for each copolymer, namely −43.2 °C for PEO–PECH5, −33.64 °C for PEO–PECH15 and −32.84 °C for PEO–PECH30. This observation of a single T_g is consistent with the fact that PEO and PECH are miscible at all volume fractions.[27,28] Furthermore, the shift

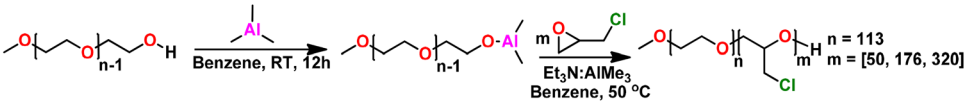

Scheme 1 Synthesis of PEO-*co*-PECH block copolymers.

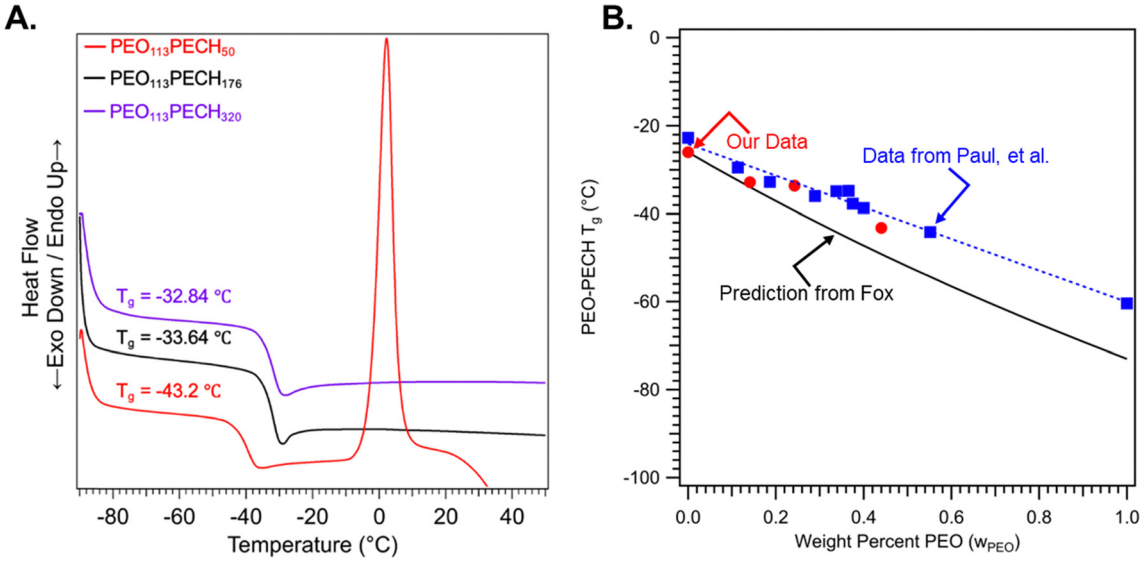

Fig. 1 (A) Truncated DSC trace of PEO-*co*-PECH block copolymers, revealing one T_g for each polymer, namely −43.2 °C for PEO–PECH5, −33.64 °C for PEO–PECH15 and −32.84 °C for PEO–PECH30. At lower molecular weights, the copolymer appears semi-crystalline (T_c = −12 °C and T_m = 49 °C). (B) T_g data as a function of w_{PEO}. The black line is the prediction from the Fox equation, the blue data is from Paul *et al.* for PEO and PECH blends, and the red data is measured from this work.

in T_g with relative PECH size to higher T_g (*i.e.*, closer to PECH T_g) is consistent with the increased fraction of PECH in the copolymer. At lower molecular weights (and smaller PECH block size), the copolymer appears semi-crystalline (T_c = 0 °C and T_m = 50 °C), with a calculated %crystallinity of 23.5% consistent with the literature.[28] At higher PECH M_n, no crystallization was observed likely due to the plasticization effect of the PECH, again consistent with the literature. To further analyze these thermal data, the T_g shift as a function of weight fraction of PEO (w_{PEO}) was calculated using the Fox equation. Fig. 1(B) contains the results from the Fox equation, as well as our data and data from Don Paul and co-workers of PEO–PECH blends. It should be noted that for Paul's work, they used a much higher molecular weight PEO, resulting in a higher T_g for w_{PEO} = 1. We adjusted our w_{PEO} for the PEO–PECH5 point based on the measured PEO crystallinity. Our measured values fall between the Fox equation prediction and Paul's experimental data and are generally close to both lines for all points.

Functionalization of polymer with iodine

PEO–PECHX were functionalized with iodine moieties to form biocompatible polymers with tunable radiopacity (iodine content). Briefly, PEO–PECHX were dissolved in MEK followed by the addition of TBAB and NaI. The reaction mixture was stirred and refluxed for 72 hours. After purification by dialysis and drying under vacuum, iodinated polymers PEO–PEI were characterized by ^{1}H NMR spectroscopy, DSC, and SEC.

The reaction scheme and truncated ^{1}H NMR spectra for PEO–PECH30 and its iodinated counterpart can be seen in Fig. 2. Full ^{1}H NMR spectra for each iodinated polymer can be found in the SI (Fig. S11–S13). The ^{1}H NMR spectra post-iodine functionalization confirmed the substitution of chlorine as a new peak emerged around 3.4 ppm representing the $\mathbf{CH_2}$–I peak with upfield shifting due to the decrease in shielding from the iodine moieties, consistent with literature.[29] Conversion of Cl to I was calculated from ^{1}H NMR spectra. An example of this calculation can be found in the SI. Conversions were 27% for PEO–PECH5, 26% for PEO–PECH15 and 92% for PEO–PECH30. While iodination reactions were performed in identical experimental conditions, the conversions were significantly lower for lower M_n polymers, however the range of substitution is consistent with the literature.[29] This difference in iodine conversion could be due to the higher relative ratio of ECH units pushing the reaction to conversion as has been observed in other examples of Finkelstein reactions.[30] Nonetheless, PEO with increasing and distinct iodine concentrations were synthesized.

PEO–PEI15 and PEO–PEI30 were analyzed *via* SEC to ensure there was no degradation of the polymer. A report of polyepiiodohydrin synthesis from the Finkelstein reaction of PECH with NaI from 1978 reported a reduction in M_n at increased iodine conversion.[29] They attributed this to cleavage of ether linkages and noted a drastic drop in molecular weight on the SEC. In our case, it is unlikely ether cleavage is occurring given the (modest) increases in M_n of our polymer noted from our SEC data. SEC traces can be found in the SI (Fig. S17 and S18). The measured M_n of PEO–PEI15 was 25.4 kg mol^{-1} and the M_n of PEO–PEI30 was 37.3 kg mol^{-1}. As such, we found small increases in polymer M_n after substitution as determined by SEC due to the limited volume change of the polymer after iodine substitution. This is expected as the absolute volume of our polymer would not change much with iodine incorporation, meaning there would be a small effect on elution time and therefore calculated molecular weight. Here, the SEC is being utilizing to confirm that our polymer is not degrading rather than to provide a way to quantify iodine substitution.

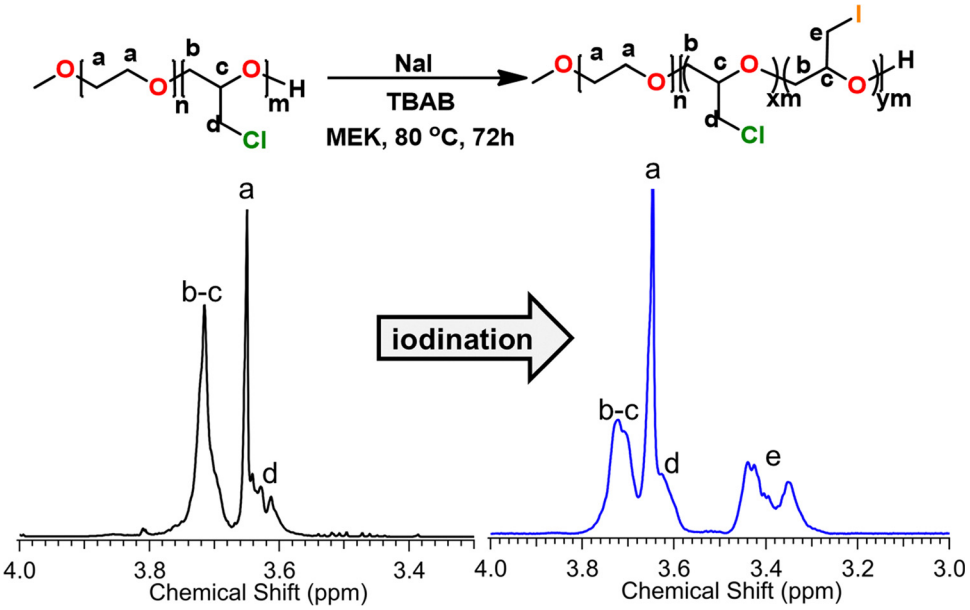

Fig. 2 (top) Reaction scheme for iodinating copolymers and ^{1}H NMR spectra of PEO–PECH30 (left) and PEO–PEI30 (right).

DSC was performed on all iodinated polymers to examine changes in thermal properties and further investigate the modification of polymer structure. T_g shifted to higher temperatures after iodination, which can be seen for the PEO–PECH5 copolymer in Fig. 3 and for the other copolymers in the SI (Fig. S14–S16) T_g = −36.9 °C for PEO–PEI5, −31.12 °C for PEO–PEI15, and −16.88 °C for PEO–PEI30. More significant shifts in T_g were observed after iodinating PEO–PECH5 (+6.3 °C) and PEO–PECH30 (+16.8 °C); however, only a small shift was observed in the PEO–PECH15 polymer (+1.72 °C).

To better understand this thermal data, we calculated the glass transition temperature of PEO–PEI polymers. A previous report produced iodinated PECH at various conversions and determined the T_g.[29] A reproduction of their glass transition data as a function of conversion can be seen in SI (Fig. S19 or Fig. 5 in ref. 29). A linear regression reveals the T_g of pure polyepiiodohydrin (*i.e.*, PECH at 100% iodine conversion) to be 10 °C. Utilizing this linear regression model, we hypothesize that the T_g at a given conversion of iodine for PECH can be predicted. This is combined with the Fox equation to predict the T_g at the calculated iodine conversion for the PEO–PEI polymers. It should be noted that the Fox equation utilizes weight fractions of the polymers and so these fractions need to be adjusted due to the increased weight of the iodinated polymers compared with neat PECH. Table 2 summarizes the data for these calculations. Here, the calculated T_g are within a few °C for PEO–PEI5 and PEO–PEI15 but is 15 °C off for PEO–PEI30. This could be due to an over-adjustment of the w_{PEO} given the increased mass of the iodinated polymers or it could be due to an overestimation of the iodination in our system

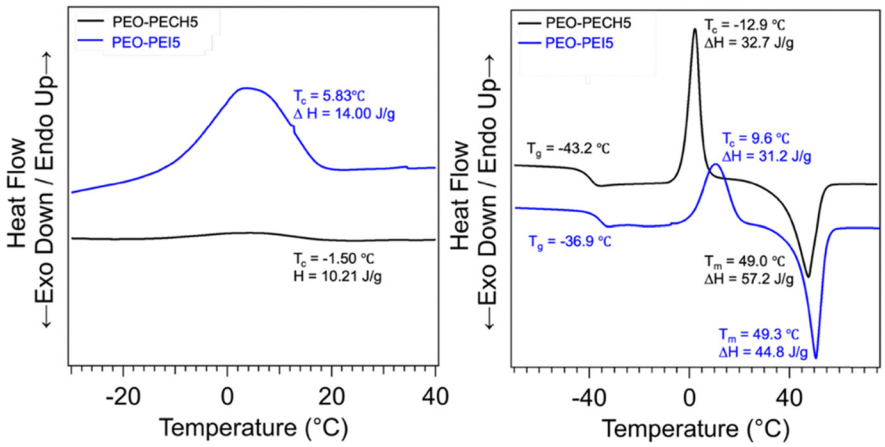

Fig. 3 DSC traces of PEO–PECH5 (black) and PEO–PEI5 (blue) showing the cooling curve (left) and the heating curve (right). The cooling curve reveals a shift in T_c after iodinating from −1.50 °C to 5.83 °C. The degree of crystallization decreased after iodinating, evidenced by the decreased change in enthalpy of crystallization. The heating curve reveals a shift in T_g by +6.3 °C, a shift in T_c from −12.9 °C to 9.6 °C, and T_m remains around 49 °C.

Table 2 Summary of calculated and measured thermal data and iodine conversion for PEO–PEI

Sample	Measured T_g[a]	Measured Conv.[b] (%)	Calculated T_g	Calculated Conv.
PEO–PEI5	−36.9	27	−41.5	45
PEO–PEI15	−31.1	26	−30.7	24
PEO–PEI30	−16.0	92	−1.0	52

[a] From DSC. [b] From ^{1}H NMR spectroscopy.

from the NMR spectrum. For completeness, we used this model to calculate the iodine conversion for each of our polymers given the measured T_g, which can be seen in Table 2. As expected, the iodine conversion is calculated to be a little higher for PEO–PEI5 and a little lower for PEO–PEI30. Our current hypothesis for this discrepancy is uncertainty in the dependence of T_g on iodine incorporation in our block-*co*-polymer structure, which is a fundamentally different material than the one from the report in 1978. In future work, we will make rigorous changes to iodine conversion and investigate the connection between composition and thermal properties.

Effect of molecular weight on cytotoxicity

Cytotoxicity of polymers was assessed in human renal proximal tubule epithelial cells and cell viability measured one-hour post exposure by fluorescence. One hour was chosen to assess acute exposure of cells to iodine, which is consistent with a clinical basis. A two-hour exposure was also done, but the trends in the data were not different than the one-hour exposure. As such, only the one-hour data is presented for clarity. Both non-iodinated (*e.g.*, PEO–PECH) and iodinated (*e.g.*, PEO–PEI) polymers were investigated as well as iohexol. A control sample was also tested with no polymer/iohexol. Fig. 4(a) is a plot of fluorescence as a function of iodine concentration for the three PEO–PEI and iohexol. Here, the iodine concentration for the polymers was calculated from the iodine conversion, polymer molecular weight, and polymer concentration. To do this, we took the polymer concentration used in the experiment (recorded as mg mL^{-1}), divided by the polymer molecular weight (in g mol^{-1}), then multiplied by the number of ECH repeat units and the percent conversion. A similar calculation was performed for iohexol. From the plot, we can see that iohexol and PEO–PEI5 behave similarly, resulting in increased cell death as a function of concentration. However, PEO–PEI15 and PEO–PEI30 show excellent cell viability, despite similar iodine concentrations. Comparing the cell viability of the iodinated polymers to the non-iodinated polymers in Fig. 4(b), we see that cell viability does not appreciably change based on polymer iodination. Rather, the polymer size seems to play an important role, as larger molecular weight polymers (*e.g.*, 15 kg mol^{-1} and 30 kg mol^{-1} PECH/PEI blocks) show excellent cell viability. The highest concentration tested for PEO–PEI30 was ∼50 mM [iodine], which corresponds to an estimated radiopacity of ∼350 HU, well within the working range for clinical CT.

We recontextualized the data as a half minimal cytotoxic concentration (CC50) to better understand the cytotoxic effects of the polymers/iohexol. CC50 was determined from a fit to the fluorescence response data. The CC50 for the PEO–PECH/PEI15/30 is not very meaningful given the lack of inhibition of fluorescence (*i.e.*, survivability of the cells). As such, the CC50 determined from a fit to the data is either unrealistically high

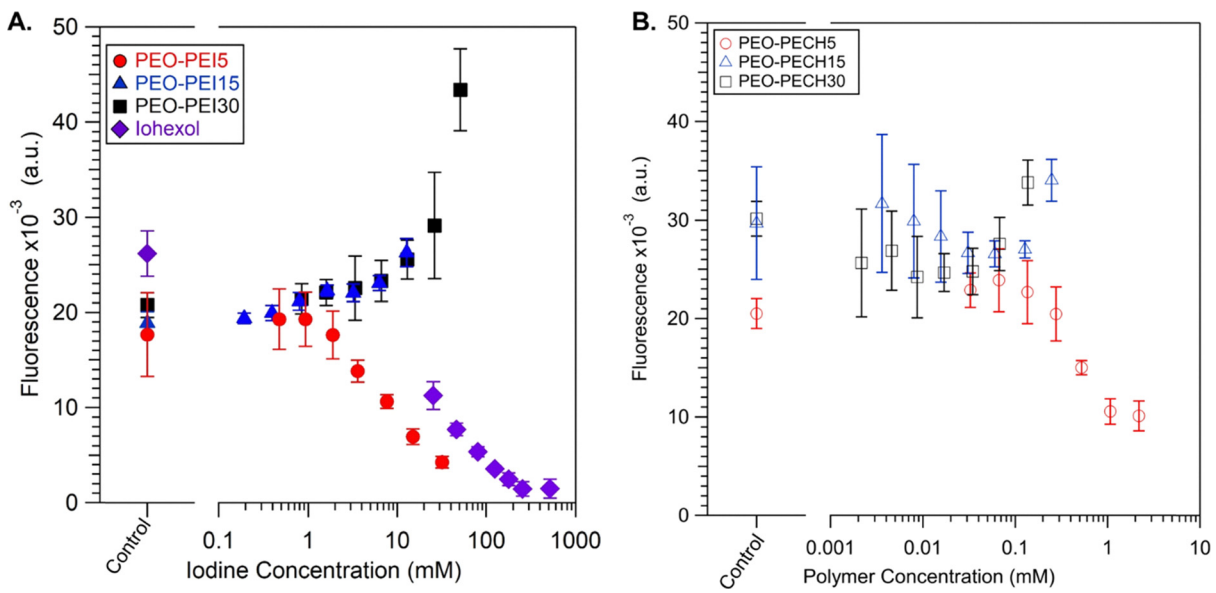

Fig. 4 (A) Fluorescence data as a function of iodine concentration from the iodinated polymers and iohexol. PEO–PECH5 has similar cytotoxicity to iohexol as marked by the decrease in cell viability after one hour of incubation. However, higher molecular weight polymers result in better cell survivability even at similar iodine concentrations to PEO–PECH5 and iohexol. (B) Fluorescence as a function of polymer concentration for non-iodinated (*e.g.*, PEO–PECH) polymers. Juxtaposing Figures A and B, we see similar trends in terms of cell viability as a function of molecular weight. In all cases, the control is with no polymer/iohexol.

or incalculable. On the other hand, the CC50 for the PEO–PECH/I5 and iohexol is meaningful. First, the CC50 for PEO–PECH5 and PEO–PEI5 are almost identical to one another, calculated to be 0.46 mM and 0.49 mM, respectively. This means that incorporation of the iodine is not appreciably affecting the toxicity of the cells, further highlighting the relation of polymer size to cytotoxicity. The iohexol had a calculated CC50 of 19.72 mM. Given that the iodinated polymers show a negligible difference in behavior in CC50 from the non-iodinated polymers, it is difficult to compare the polymer CC50 to the iohexol CC50. For instance, what concentrations do we compare? Since PEO is generally viewed as non-cytotoxic, we could recalculate the CC50 of PEO–PECH5 in terms of ECH units. In this case, the CC50 of ECH is 24.86 mM, similar to iohexol. This comparison is likely dubious given at higher ECH concentrations (*i.e.*, PEO–PECH15/30) we see limited cytotoxicity. Further studies need to be done to better understand the source of cytotoxicity with the smaller polymers.

Lower molecular weight polymers exhibited greater toxicity with behavior similar to that of iohexol. Khanh *et al.* found a strong correlation between PEO molecular weight and cytotoxicity, with cytotoxicity decreasing as PEO chain length was increased.[31] Postic *et al.* investigated the effect of PEO molecular weight on cell viability and cell morphology and similarly found that high concentrations of low molecular weight PEOs were more cytotoxic and prompted significant changes in cell morphology compared to high molecular weight PEOs.[32] Cell death was attributed to the mechanism of cellular uptake of low molecular weight PEOs (passive diffusion) *vs.* endocytosis for longer chain PEOs.[33] The toxic effects observed in the aforementioned works were in PEG with molecular weights much smaller than ours (*ca.* 200 g mol^{-1}) and large sets of data support the benign nature of cells towards PEG/PEO at higher molecular weights.

PECH has received limited study in relation to cytotoxicity. Our initial intuition was that PECH would be cytotoxic, and we hoped that the PEO block would mitigate this. However, the limited literature data supports that higher molecular weight PECH and PEO/PECH copolymers are benign.[34,35] However, there is some evidence that low molecular weight/oligomeric PECH is cytotoxic.[36] Given the results with lower MW PEO–PECH (*i.e.*, 5 kg mol^{-1}) being cytotoxic and higher M_n not, this is generally consistent with the literature. As such, our work further establishes the effect of PEG and PEG derivatives molecular weight on cell viability.

X-Ray attenuation of iodinated polymers

X-Ray attenuation was measured for PEO–PEI5 and compared to iohexol, a standard contrast agent. μCT imaging of PEO–PEI5 in DI water was performed in a range of sample concentrations up to 25 mM and compared to iohexol up to 500 mM. The images in Fig. 5(A) show clearly effective attenuation with PEO–PEI5 at concentrations less than 25 mM while the iohexol requires significantly higher concentrations (between 250 and 500 mM). The incorporation of ultra-high amounts of iodine on the PEO backbone in comparison to iohexol allows for high X-ray attenuation at significantly lower sample concentrations. These results were observed in PEO–PEI5 and we expect that increased conversion or increasing PECH chain length should result in increased attenuation at even lower sample concentrations. If we instead consider a wt% approach, 12.5 mM PEO–PEI5 is *ca.* 11 wt% while 250 mM iohexol is *ca.* 29 wt%, indicating even on a per weight basis X-ray attenuation is improved with the polymer. That being said, as is shown in Fig. 5(B), on a per iodine basis, the response between the polymer and conventional contrast agent iohexol is similar, as explained in the subsequent paragraph.

The iodine content in the PEO–PEI5 and iohexol was measured at each of the concentrations in the CT experiments by ICP-MS. The X-ray attenuation was then plotted as a function of the measured iodine content as can be seen in Fig. 5(B). Radiopacity scales linearly with iodine content, in agreement

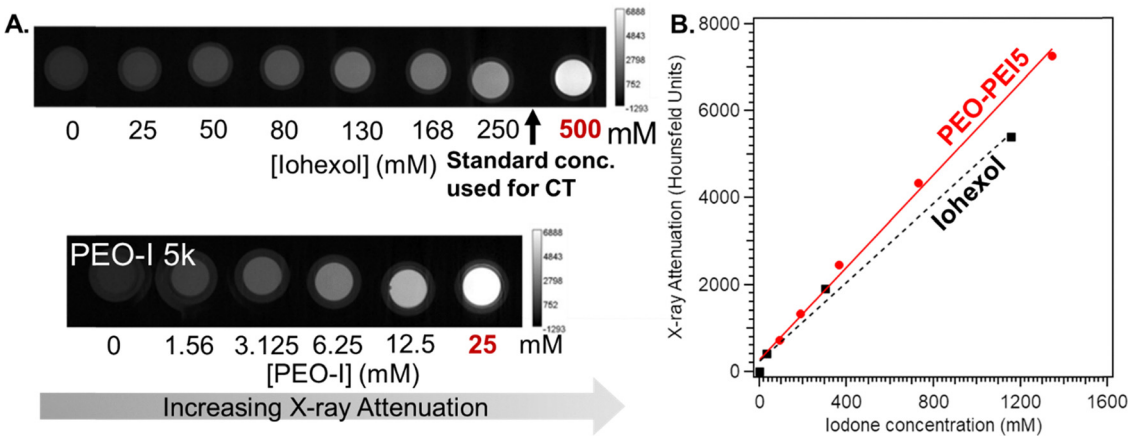

Fig. 5 (A) Micro CT images of iohexol (top) and PEO–PEI5 (bottom) in DI water in a range of sample concentrations. Effective attenuation is achieved at 12.5 mM of PEO–PEI5 compared to 250 mM of iohexol, a 20× concentration difference. In terms of wt%, this translates to 11 wt% for PEO–PEI5 and 29 wt% for iohexol. (B) Plot of X-ray attenuation as a function of iodine concentration for PEO–PEI5 and Iohexol with lines with linear regression fits showing similar trends in X-ray attenuation.

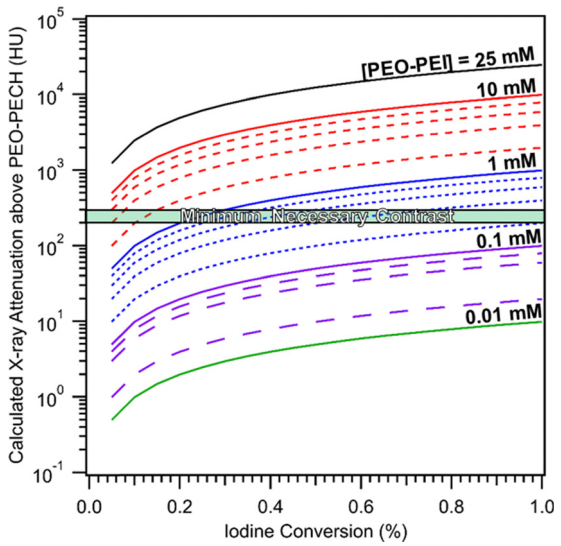

Fig. 6 Predicted X-ray attenuation given iodine conversion for a range of polymer concentrations for PEO–PEI15. The green bar shows the minimum necessary contrast to distinguish features from surrounding media *in vivo*.

with literature.[37] This imaging trend aligns with other studies using different radiopaque elements.[38,39] The slopes for iodinated PEO (PEO–PEI5) and iohexol were 5.6 HU mM^{-1} iodine and 4.8 HU mM^{-1} iodine respectively, which were not significantly different. These results confirm the tunability of X-ray attenuation due to the block copolymer system in which this work is based on. From the fits to the above data and given the amount of iodine attached to the PECH–PEI, we generated a predictive model for the X-ray attenuation given polymer concentration at a particular $Cl^- >$ I conversion, which can be found in Fig. 6. From this data, we see a discrepancy between the conversion calculated conversion and the amount of iodine present.

The maximum number of iodine bound to the polymer sample depends on the size of the precursor PECH block and $Cl^- >$ I conversion, with higher molecular weights and conversion having higher iodine content. Thus, targeting larger PECH blocks should conceivably result in increased attenuation while the overall sample concentration is held constant. The radiopacity of higher molecular weight iodinated polymers was measured in DI water; however, poor solubility limited the concentration range evaluated. In this concentration range, the radiopacity of iodinated polymers was low, 124.2 ± 7.67 HU for PEO–PEI15 and 124.2 ± 12.8 HU for PEO–PEI30. This is lower than the predicted radiopacity from the model and is likely due to the poor solubility in hydrophilic solvents (*e.g.*, water and PBS buffer) as they tended to crash out of solution even at low concentrations (~5 to 12 mg mL^{-1}).

To confirm that the poor water/PBS solubility was indeed the reason for the low attenuation, X-ray attenuation was measured for PEO–PEI15 and PEO–PEI30 in DCM. Since DCM (*ca.* 1600 HU) is denser than water (0 HU), so baseline attenuations of these two solvents are different. Here, we achieved high X-ray attenuation, which we define as >300 HU above baseline (*i.e.*, 1600 HU for DCM + 300 HU ≈ 1900 HU), in polymer concentrations at or above 50 mg mL^{-1}, highlighting the importance of solubility on X-ray attenuation. X-Ray attenuation increases linearly with increasing polymer concentration (and subsequent iodine concentration) shown in Fig. S20 in the SI. As a check, we backed out the iodine concentration for these polymers (taking into account calculated iodine conversion, molecular weight, *etc.*) and replot them as HU as a function of iodine concentration, as seen in Fig. S21. We find that the curves overlap, meaning the iodine in one polymer is giving the same enhancement to contrast as iodine in the other polymer, which is what we would expect. Furthermore, this lends weight to our ^{1}H NMR spectroscopy-based calculation of iodine conversion, since if this was off, the fits would not overlap. In the future, hydrophilicity issues can be mitigated by further polymer modification. Due to the versatility of the precursor block copolymers, polymer structures can be tuned by modifying Cl pendants of the PECH block with hydrophilic moieties prior to iodinating or prepared as micelles to facilitate solubility.

Conclusion

In this work, iodinated polymers were formed from functional block copolymers consisting of PEO and PECH, which provide high tunability, high iodine content, and are non-cytotoxic. These results confirm the tunability of X-ray attenuation in PEO–PECH platforms, in which iodine concentration can be varied by increasing PECH or PEO block prior to the iodination step. Further, Cl moieties can conceivably be tuned with other desired functional groups prior to iodination, which would affect final iodine concentrations. The effect of polymer molecular weight on renal toxicity was investigated and revealed that in contrast to iohexol, cytotoxicity was dependent on polymer molecular weight rather than iodine concentration, with higher molecular weight polymers exhibiting less toxicity than low molecular weight. All iodinated polymers effectively attenuate X-rays, with PEO–PEI5 achieving effective attenuation at 11 wt% compared to iohexol at 29 wt%. Poor solubility of higher molecular weight PEO–PEI in hydrophilic media limits their clinical application as intravenous contrast agents, but does not discount them as contrast agents that can be incorporated into polymer-based biomedical devices. Further, the versatility of the block copolymer structure allows for tuning capabilities to achieve the desired properties of solubility, biocompatibility, and X-ray attenuation.

Conflicts of interest

There are no conflicts to declare.

Data availability

The data supporting this article have been included as part of the SI. Supplementary information: full NMR spectra, DSC

curves, SEC traces, X-ray attenuation data, and example calculations. See DOI: https://doi.org/10.1039/d5tb02069g.

Acknowledgements

The authors acknowledge funding from Michigan State University's TETRAD Initiative. RCF acknowledges funding through the Jenison Fund at Michigan State University.

References

1 G. N. Hounsfield, Computerized transverse axial scanning (tomography). 1. Description of system, *Br. J. Radiol.*, 1973, **46**(552), 1016–1022, DOI: 10.1259/0007-1285-46-552-1016 From NLM.
2 T. C. Owens, N. Anton and M. F. Attia, CT and X-ray contrast agents: Current clinical challenges and the future of contrast, *Acta Biomater.*, 2023, **171**, 19–36, DOI: 10.1016/j.actbio.2023.09.027.
3 N. Lee, S. H. Choi and T. Hyeon, Nano-Sized CT Contrast Agents, *Adv. Mater.*, 2013, **25**(19), 2641–2660, DOI: 10.1002/adma.201300081.
4 L. Caschera, A. Lazzara, L. Piergallini, D. Ricci, B. Tuscano and A. Vanzulli, Contrast agents in diagnostic imaging: Present and future, *Pharmacol. Res.*, 2016, **110**, 65–75, DOI: 10.1016/j.phrs.2016.04.023.
5 H. Lusic and M. W. Grinstaff, X-ray-Computed Tomography Contrast Agents, *Chem. Rev.*, 2013, **113**(3), 1641–1666, DOI: 10.1021/cr200358s.
6 F. Stacul, Current iodinated contrast media, *Eur. Radiol.*, 2001, **11**(4), 690–697, DOI: 10.1007/s003300000620.
7 A.-L. Faucon, G. Bobrie and O. Clément, Nephrotoxicity of iodinated contrast media: From pathophysiology to prevention strategies, *Eur. J. Radiol.*, 2019, **116**, 231–241, DOI: 10.1016/j.ejrad.2019.03.008.
8 A. J. van der Molen, H. S. Thomsen and S. K. Morcos, Members of Contrast Media Safety Committee of European Society of Urogenital, R. Effect of iodinated contrast media on thyroid function in adults, *Eur. Radiol.*, 2004, **14**(5), 902–907, DOI: 10.1007/s00330-004-2238-z.
9 T. G. Maddox, Adverse reactions to contrast material: recognition, prevention, and treatment, *Am. Fam. Physician*, 2002, **66**(7), 1229–1234 From NLM.
10 J. Zhang, W. Liu, P. Zhang, Y. Song, Z. Ye, H. Fu, S. Yang, Q. Qin, Z. Guo and J. Zhang, Polymers for Improved Delivery of Iodinated Contrast Agents, *ACS Biomater. Sci. Eng.*, 2022, **8**(1), 32–53, DOI: 10.1021/acsbiomaterials.1c01082.
11 V. P. Torchilin, PEG-based micelles as carriers of contrast agents for different imaging modalities, *Adv. Drug Delivery Rev.*, 2002, **54**(2), 235–252, DOI: 10.1016/S0169-409X(02)00019-4.
12 V. S. Trubetskoy, Polymeric micelles as carriers of diagnostic agents, *Adv. Drug Delivery Rev.*, 1999, **37**(1), 81–88, DOI: 10.1016/S0169-409X(98)00100-8.
13 Y. Zou, Y. Wei, G. Wang, F. Meng, M. Gao, G. Storm and Z. Zhong, Nanopolymersomes with an Ultrahigh Iodine Content for High-Performance X-Ray Computed Tomography Imaging *In Vivo*, *Adv. Mater.*, 2017, **29**(10), 1603997, DOI: 10.1002/adma.201603997.
14 C. Tang, A. W. York, J. L. Mikitsh, A. C. Wright, A.-M. Chacko, D. R. Elias, Y. Xu, H.-K. Lim and R. K. Prud'homme, Preparation of PEGylated Iodine-Loaded Nanoparticles via Polymer-Directed Self-Assembly, *Macromol. Chem. Phys.*, 2018, **219**(11), 1700592, DOI: 10.1002/macp.201700592.
15 P. Ghosh, M. Das, A. P. Rameshbabu, D. Das, S. Datta, S. Pal, A. B. Panda and S. Dhara, Chitosan Derivatives Cross-Linked with Iodinated 2,5-Dimethoxy-2,5-dihydrofuran for Non-Invasive Imaging, *ACS Appl. Mater. Interfaces*, 2014, **6**(20), 17926–17936, DOI: 10.1021/am504655v.
16 K. M. Pawelec, S. Chakravarty, J. M. L. Hix, K. L. Perry, L. van Holsbeeck, R. Fajardo and E. M. Shapiro, Design Considerations to Facilitate Clinical Radiological Evaluation of Implantable Biomedical Structures, *ACS Biomater. Sci. Eng.*, 2021, **7**(2), 718–726, DOI: 10.1021/acsbiomaterials.0c01439.
17 K. M. Pawelec, J. M. L. Hix, A. Troia, K. W. MacRenaris, M. Kiupel and E. M. Shapiro, *In vivo* micro-computed tomography evaluation of radiopaque, polymeric device degradation in normal and inflammatory environments, *Acta Biomater.*, 2024, **181**, 222–234, DOI: 10.1016/j.actbio.2024.04.031.
18 O. Rabin, J. Manuel Perez, J. Grimm, G. Wojtkiewicz and R. Weissleder, An X-ray computed tomography imaging agent based on long-circulating bismuth sulphide nanoparticles, *Nat. Mater.*, 2006, **5**(2), 118–122, DOI: 10.1038/nmat1571.
19 R. Popovtzer, A. Agrawal, N. A. Kotov, A. Popovtzer, J. Balter, T. E. Carey and R. Kopelman, Targeted Gold Nanoparticles Enable Molecular CT Imaging of Cancer, *Nano Lett.*, 2008, **8**(12), 4593–4596, DOI: 10.1021/nl8029114.
20 I. Mutreja, N. Maalej, A. Kaushik, D. Kumar and A. Raja, High atomic number nanoparticles to enhance spectral CT imaging aspects, *Mater. Adv.*, 2023, **4**(18), 3967–3988, DOI: 10.1039/D3MA00231D.
21 R. C. Ferrier Jr., J. Koski, R. A. Riggleman and R. J. Composto, Engineering the Assembly of Gold Nanorods in Polymer Matrices, *Macromolecules*, 2016, **49**(3), 1002–1015, DOI: 10.1021/acs.macromol.5b02317.
22 S. K. Kumar, N. Jouault, B. Benicewicz and T. Neely, Nanocomposites with Polymer Grafted Nanoparticles, *Macromolecules*, 2013, **46**(9), 3199–3214, DOI: 10.1021/ma4001385.
23 J. Imbrogno, R. C. Ferrier, B. K. Wheatle, M. J. Rose and N. A. Lynd, Decoupling Catalysis and Chain-Growth Functions of Mono(μ-alkoxo)bis(alkylaluminums) in Epoxide Polymerization: Emergence of the N–Al Adduct Catalyst, *ACS Catal.*, 2018, **8**(9), 8796–8803, DOI: 10.1021/acscatal.8b02446.
24 N. Safaie, B. Rawal, K. Ohno and R. C. Ferrier, Aluminum-Based Initiators from Thiols for Epoxide Polymerizations,

Macromolecules, 2020, **53**(19), 8181–8191, DOI: 10.1021/acs.macromol.0c00464.

25 N. Safaie, J. Smak, D. DeJonge, S. Cheng, X. Zuo, K. Ohno and R. C. Ferrier, Facile synthesis of epoxide-*co*-propylene sulphide polymers with compositional and architectural control, *Polym. Chem.*, 2022, **13**(19), 2803–2812, DOI: 10.1039/D2PY00005A.

26 J. M. Keever, B. J. Pedretti, Z. W. Brotherton, J. Imbrogno, Y. Kataoka, J. Baltzegar, N. Kambayashi and N. A. Lynd, Chain extension epoxide polymerization to well-defined block polymers using a N-Al Lewis pair catalyst, *J. Polym. Sci.*, 2024, **62**(11), 2527–2538, DOI: 10.1002/pol.20240002.

27 A. C. Fernandes, J. W. Barlow and D. R. Paul, Blends containing polymers of epichlorohydrin and ethylene oxide. Part I: Polymethacrylates, *J. Appl. Polym. Sci.*, 1986, **32**(6), 5481–5508, DOI: 10.1002/app.1986.070320618.

28 K. E. Min, J. S. Chiou, J. W. Barlow and D. R. Paul, A completely miscible ternary blend: poly(methyl methacrylate)-poly(epichlorohydrin)-poly(ethylene oxide, *Polymer*, 1987, **28**(10), 1721–1728, DOI: 10.1016/0032-3861(87)90016-4.

29 E. Schacht, D. Bailey and O. Vogl, Polyepiiodohydrin, *J. Polym. Sci., Polym. Chem. Ed.*, 1978, **16**(9), 2343–2351, DOI: 10.1002/pol.1978.170160921.

30 R. D. Pace and Y. Regmi, The Finkelstein Reaction: Quantitative Reaction Kinetics of an SN2 Reaction Using Nonaqueous Conductivity, *J. Chem. Educ.*, 2006, **83**(9), 1344, DOI: 10.1021/ed083p1344.

31 H. Pham Le Khanh, D. Nemes, Á. Rusznyák, Z. Ujhelyi, P. Fehér, F. Fenyvesi, J. Váradi, M. Vecsernyés and I. Bácskay, Comparative Investigation of Cellular Effects of Polyethylene Glycol (PEG) Derivatives, *Polymers*, 2022, **14**(2), 279.

32 I. Postic and H. Sheardown, Poly(ethylene glycol) induces cell toxicity in melanoma cells by producing a hyperosmotic extracellular medium, *J. Biomater. Appl.*, 2018, **33**(5), 693–706, DOI: 10.1177/0885328218807675.

33 T. Wang, Y. Guo, Y. He, T. Ren, L. Yin, J. P. Fawcett, J. Gu and H. Sun, Impact of molecular weight on the mechanism of cellular uptake of polyethylene glycols (PEGs) with particular reference to P-glycoprotein, *Acta Pharm. Sin. B*, 2020, **10**(10), 2002–2009, DOI: 10.1016/j.apsb.2020.02.001.

34 N. Mamidi, H. M. L. Gutiérrez, J. Villela-Castrejón, L. Isenhart, E. V. Barrera and A. Elías-Zúñiga, Fabrication of gelatin-poly(epichlorohydrin-*co*-ethylene oxide) fiber scaffolds by Forcespinning® for tissue engineering and drug release, *MRS Commun.*, 2017, **7**(4), 913–921, DOI: 10.1557/mrc.2017.117.

35 N. L. G. D. Souza, M. Munk, H. M. Brandão and L. F. C. de Oliveira, Functionalization of poly(epichlorohydrin) using sodium hydrogen squarate: cytotoxicity and compatibility in blends with chitosan, *Polym. Bull.*, 2018, **75**(10), 4627–4639, DOI: 10.1007/s00289-018-2290-5.

36 S. Zhou, X. Xu, N. Ma, F. Jung and A. Lendlein, Prediction of the epichlorohydrin derived cytotoxic substances from the eluent of poly(glycerol glycidyl ether) films, *MRS Adv.*, 2022, **7**(16), 354–359, DOI: 10.1557/s43580-021-00132-y.

37 K. Kolouchova, Q. Thijssen, O. Groborz, L. Van Damme, J. Humajova, P. Matous, A. Quaak, M. Dusa, J. Kucka, L. Sefc, M. Hruby and S. Van Vlierberghe, Next-Gen Poly(ε-Caprolactone) Scaffolds: Non-Destructive *In Vivo* Monitoring and Accelerated Biodegradation, *Adv. Healthcare Mater.*, 2025, **14**(1), e2402256, DOI: 10.1002/adhm.202402256 From NLM.

38 J. Kim, D. Bar-Ness, S. Si-Mohamed, P. Coulon, I. Blevis, P. Douek and D. P. Cormode, Assessment of candidate elements for development of spectral photon-counting CT specific contrast agents, *Sci. Rep.*, 2018, **8**(1), 12119, DOI: 10.1038/s41598-018-30570-y.

39 K. M. Pawelec, J. M. L. Hix, M. Kiupel, P. J. Bonitatibus Jr and E. M. Shapiro, Hydrophilic Particles Exit While Hydrophobic Particles Persist Following *In Vivo* Biodegradation of Nanoparticle-Laden Polymeric Devices, *Adv. NanoBiomed Res.*, 2025, **5**(6), 2500005, DOI: 10.1002/anbr.202500005 (acccessed 2025/11/24).

